



13th World Conference on Earthquake Engineering
Vancouver, B.C., Canada
August 1-6, 2004
Paper No. 547

PSEUDO-THREE DIMENSIONAL LAGRANGIAN PARTICLE FINITE DIFFERENCE METHOD FOR MODELING EARTHQUAKE-INDUCED SOIL FLOWS

Kazuo KONAGAI¹, Jörgen JOHANSSON² and Hironori ITOH³

SUMMARY

Landslides can range in size from small movements of loose debris to massive collapses of entire summits. For short to medium-length slopes, some measures will be effective for assessing and mitigating landslide hazards. Extremely large slope failures, however, are very difficult to mitigate, and the importance of run-out analysis emerges. Lagrangian Particle Finite Difference Method (LPFDM) is extended to handle rapid and long-traveling flows of soil. LPFDM describes a soil mass as a cluster of Lagrangian material points that carry all necessary information of the material and move freely across a Eulerian grid where the equations of motion are solved.

INTRODUCTION

Landslides can range in size from small movements of loose debris to massive collapses of entire summits. For short to medium-length slopes, installing preventive drainage works, anchoring and/or reinforcing slopes will be effective for assessing and mitigating landslide hazards. Extremely large slope failures, however, are very difficult to mitigate, and thus the importance of run-out analysis emerges. Many landslides with limited internal deformation will move as coherent masses on thin mobile basal layers. Others, however, will become flow-like in character after running some long distances, though exhibiting some solid features at their early stages of failure.

For studying large deformations of soils, numerical methods such as FEM or FDM have been widely used. For example, the finite difference based FLAC (Fast Lagrangian Analysis of Continua) [1] calculates large strains by using low-order strain elements. However, when dealing with large strains, highly distorted elements often account for inaccurate results.

¹ Professor, Institute of Industrial Science, University of Tokyo, Japan. Email: konagai@iis.u-tokyo.ac.jp

² Associate Researcher, ditto. Email: jorgen@iis.u-tokyo.ac.jp

³ Graduate Student, ditto. Email: itouhnr@iis.u-tokyo.ac.jp

In the field of computational fluid dynamics, where history-dependent materials are less common, purely Eulerian methods are often used. Sulsky et al. [2] extended one of these methods to solid mechanics. Their method evolved from a particle-in-cell (PIC) method is referred to as the Material Point Method (MPM) and is categorized as a mesh-less method. In MPM, a body to be analyzed is described as a cluster of material points. The material points, which carry all Lagrangian parameters, can move freely across cell boundaries of a stationary Eulerian computational mesh, which should cover the position of the analyzed body. The computational mesh can remain constant for the entire computation, thus the large deformation disadvantage of the conventional finite element method related to the problem of mesh distortions is eliminated.

Konagai and Johansson [3] developed two-dimensional LPFDM (Lagrangian Particle Finite Difference Method) based on simple finite difference scheme of calculation, but with the inclusion of lagrangian particles/ material points. The method is intended to be a combination of the schemes of FLAC and MPM so that the present method allows for extremely large deformations of soils retaining the simplicity of FLAC. The method is further extended herein to model a rapid and long-traveling soil flow keeping its planar geometry.

MODELING OF LANDSLIDE MASS

Solid phase

Though the use of a three-dimensional model is a straightforward approach to the problem, here a thin landslide mass flowing over a stiff base slope is modeled as a two-dimensional soil mat. The landslide mass consists of a plane assembly of soil columns, represented by material points, in contact with each other, free to deform and retaining fixed volumes in their descent down a curving path (**Figure 1**).

Cells of a computational Eulerian mesh on the $\xi - \psi$ plane are arranged in such a way that their projections on a horizontal x - y plane are a regular square mesh with sides parallel to x and y axes of the Cartesian coordinate system. Though the real slope is not a perfect plane, each cell is assumed to be small enough for the cell and its neighboring cells to be arranged in one plane. The cells on the $\xi - \psi$ plane are thus parallelograms. The orientation of the $\xi - \psi$ plane is described by ξ and ψ axes; the ξ axis is perpendicular to the slope direction and the ψ axis is parallel to the slope direction of the $\xi - \psi$ plane. The LPFDM formulation on the $\xi - \psi$ plane is available in Konagai et al. [4].

A soil column (material point) is assumed to experience the same strains in the $\xi - \psi$ plane over its entire height ($z: 0-h$). Excluding its weight, the stress components for the soil column, $\sigma_{xx,0}$, $\sigma_{yy,0}$ and $\tau_{xy,0}$ are kept unchanged over its height. However with the presence of its weight, realized stress components are described as:

$$\sigma_{xx} = \sigma_{xx,0} + K_0 \gamma z, \quad \sigma_{yy} = \sigma_{yy,0} + K_0 \gamma z, \quad \tau_{xy} = \tau_{xy,0} \quad \sigma_{zz} = \gamma z, \quad \text{with } K_0 = \frac{\nu}{1-\nu} \quad (1)$$

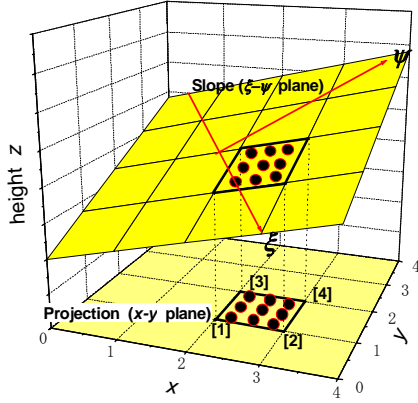


Figure 1. Material points on a slip surface

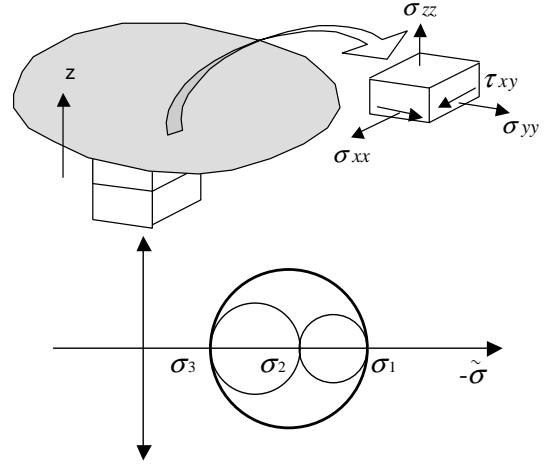


Figure 2. Soil column (above) following Mohr-Coulomb's criterion (below)

The above components are averaged over the column's height.

$$\begin{aligned}\tilde{\sigma}_{xx} &= \frac{1}{h} \int_0^h \sigma_{xx} dz = \sigma_{xx,0} + \frac{1}{2} K_0 \gamma h, \quad \tilde{\sigma}_{yy} = \frac{1}{h} \int_0^h \sigma_{yy} dz = \sigma_{yy,0} + \frac{1}{2} K_0 \gamma h, \quad \tilde{\tau}_{xy} = \tau_{xy,0} \\ \text{and } \tilde{\sigma}_{zz} &= \frac{1}{h} \int_0^h \sigma_{zz} dz = \frac{1}{2} \gamma h\end{aligned}\quad (2a)-(2d)$$

Essentially, Mohr/Coulomb criterion should be used for a particular soil element that experiences homogeneous stresses over its entire size. For the averaged stress components, however, Mohr/Coulomb criterion is tentatively used herein for describing elasto-plastic features of the “material point”. To draw a Mohr circle for the material point, the maximum and minimum principal stresses must be chosen among three principal stresses including $\tilde{\sigma}_{zz}$. For this, two principal stresses $\tilde{\sigma}_a$ and $\tilde{\sigma}_b$ in the x - y plane are first to be obtained. It is noted that differing from the geotechnical engineering customary to describe compressive stresses as positive, tensile stresses are expressed to be positive in LPFDM.

$$\tilde{\sigma}_a = \left(\frac{\tilde{\sigma}_{xx} + \tilde{\sigma}_{yy}}{2} + \sqrt{\left(\frac{\tilde{\sigma}_{xx} - \tilde{\sigma}_{yy}}{2} \right)^2 + \tilde{\tau}_{xy}^2} \right) = \left(\frac{\sigma_{xx,0} + \sigma_{yy,0}}{2} + \sqrt{\left(\frac{\sigma_{xx,0} - \sigma_{yy,0}}{2} \right)^2 + \tau_{xy,0}^2} \right) + \frac{1}{2} \gamma h \quad (3a)$$

$$\tilde{\sigma}_b = \left(\frac{\sigma_{xx,0} + \sigma_{yy,0}}{2} - \sqrt{\left(\frac{\sigma_{xx,0} - \sigma_{yy,0}}{2} \right)^2 + \tau_{xy,0}^2} \right) + \frac{1}{2} \gamma h \quad (3b)$$

Among the three principal stresses, the maximum, intermediate and minimum principal stresses are determined as:

$$\begin{aligned}\sigma_1 &= \max(-\tilde{\sigma}_a, -\tilde{\sigma}_b, -\tilde{\sigma}_{zz}), \quad \sigma_2 = \text{intermediate}(-\tilde{\sigma}_a, -\tilde{\sigma}_b, -\tilde{\sigma}_{zz}) \\ \text{and } \sigma_3 &= \min(-\tilde{\sigma}_a, -\tilde{\sigma}_b, -\tilde{\sigma}_{zz}).\end{aligned}\quad (4a), (4b), (4c)$$

i.e. one of the principal stresses is always assumed to be in the vertical direction. Once the Mohr circle intersects the failure envelope, stresses are “reduced” in such a way that the reduced stress make up a slightly reduced Mohr circle that touches the envelope.

Liquid phase

Soils are often moist, and thus pore-water behavior should be taken appropriately into account. In the present program, only a two-dimensional flow of water through a saturated plane landslide mass is considered. To account for a rapid soil flow, the water flow through the granular fabric is assumed to obey Ergun's law. Not a granular fabric but its void is assumed to change its volume. In the time-marching calculation, an element size should satisfy the following condition:

$$v_L \Delta t \ll L \quad (5)$$

where

Δt = time increment and L = cell size

It is customary in geotechnical engineering to describe compressive pressure as positive. But notation here follows the conventional way for FEM formulations, and thus sucking pore pressure p is described as positive. In Lagrangian point k included in Cell J , the initial volumes of solid phase and pore-water are given respectively by:

$$V_{k,solid} = \frac{1}{1+e} (V_k)_{t=0} \quad (6a)$$

$$(\bar{V}_{k,0})_{t=0} = \frac{e}{1+e} (V_k)_{t=0} \quad (6b)$$

where, V_k is the volume of the material point k , and e is the void ratio.

A change in void causes an excessive pore pressure $\Delta \bar{p}_k$ as:

$$\Delta p_k = K \left((\bar{V}_k)_t - (\bar{V}_{k,0})_t \right) / (\bar{V}_{k,0})_t - \rho g \Delta y \quad (7a)$$

$$(\bar{V}_k)_t = (V_k)_t - V_{k,solid} \quad \text{with}$$

where

$$(V_k)_t = (V_k)_{t-\Delta t} \left(1 + \langle \Delta \epsilon_{xx} \rangle_{k \in J} \right) \cdot \left(1 + \langle \Delta \epsilon_{yy} \rangle_{k \in J} \right) \quad \text{and} \quad (7b)$$

K is the compressibility (equivalent bulk modulus) of water in the plane landslide mass. The plan flow, however, is associated with it orthogonal component normal to the slip surface. To reflect this feature on the analysis, the equivalent bulk modulus must be set at a smaller value than that for the complete plane strain case. The change of pore pressure causes pore water to flow within a plane granular fabric. Velocities of percolation in x and y directions are respectively given by the following equations (Ergun, 1952):

$$\frac{\partial \Delta p_k}{\partial x} = \left(f_1 \cdot |\bar{\mathbf{v}}| + f_2 \cdot |\bar{\mathbf{v}}|^2 \right) \cdot \frac{v_x}{|\bar{\mathbf{v}}|} \quad (8a), (8b)$$

$$\frac{\partial \Delta p_k}{\partial y} = \left(f_1 \cdot |\bar{\mathbf{v}}| + f_2 \cdot |\bar{\mathbf{v}}|^2 \right) \cdot \frac{v_y}{|\bar{\mathbf{v}}|}$$

where,

$$\bar{\mathbf{v}} = (v_x, v_y), \quad f_1 = 150 \frac{(1+e)}{e^3} \frac{\mu}{D^2}, \quad f_2 = 1.75 \frac{(1+e)^2}{e^3} \frac{\rho}{D}, \quad (8c)-(8e)$$

μ = viscosity of water, ρ = water density, and D = grain diameter.

From equations (8a) and (8b), one obtains:

$$\sqrt{\left(\frac{\partial \Delta p_k}{\partial x} \right)^2 + \left(\frac{\partial \Delta p_k}{\partial y} \right)^2} = f_1 \cdot |\bar{\mathbf{v}}| + f_2 \cdot |\bar{\mathbf{v}}|^2 \quad (9a)$$

Equation (9a) yields:

$$|\bar{v}| = -f_1 / 2f_2 + \sqrt{(f_1 / 2f_2)^2 + \frac{1}{f_2} \sqrt{\left(\frac{\partial \Delta p_k}{\partial x}\right)^2 + \left(\frac{\partial \Delta p_k}{\partial y}\right)^2}} \quad (9b)$$

Both v_x and v_y are obtained by substituting Equation (9b) in Equations (8a) and (8b) with $\partial \Delta p_k / \partial x$ and $\partial \Delta p_k / \partial y$ provided as known values. The volume of water flowing into the material point k within the time increment Δt is then given by:

$$\begin{aligned} \Delta \bar{V}_{k,0} &= -\left(\frac{\partial v_x}{\partial x} + \frac{\partial v_y}{\partial y}\right) V_k \Delta t \\ &= -\frac{V_k \Delta t}{Q} \left[\left(f_1 + f_2 \left(\frac{v_y^2}{|\bar{v}|} + |\bar{v}| \right) \right) \frac{\partial^2 \Delta p_k}{\partial x^2} - 2f_2 \frac{v_x v_y}{|\bar{v}|} \frac{\partial^2 \Delta p_k}{\partial x \partial y} + \left(f_1 + f_2 \left(\frac{v_x^2}{|\bar{v}|} + |\bar{v}| \right) \right) \frac{\partial^2 \Delta p_k}{\partial y^2} \right] \end{aligned} \quad (10)$$

With
$$Q = (f_1 + f_2 (v_x^2 / |\bar{v}| + |\bar{v}|)) \cdot (f_1 + f_2 (v_y^2 / |\bar{v}| + |\bar{v}|)) - \left(f_2 \frac{v_x v_y}{|\bar{v}|} \right)^2$$

This $\Delta \bar{V}_{k,0}$ is then added to $(\bar{V}_{k,0})_{t-\Delta t}$, and this procedure updates $\bar{V}_{k,0}$ in Equation (7a).

$$(\bar{V}_{k,0})_t = (\bar{V}_{k,0})_{t-\Delta t} + \Delta \bar{V}_{k,0} \quad (11)$$

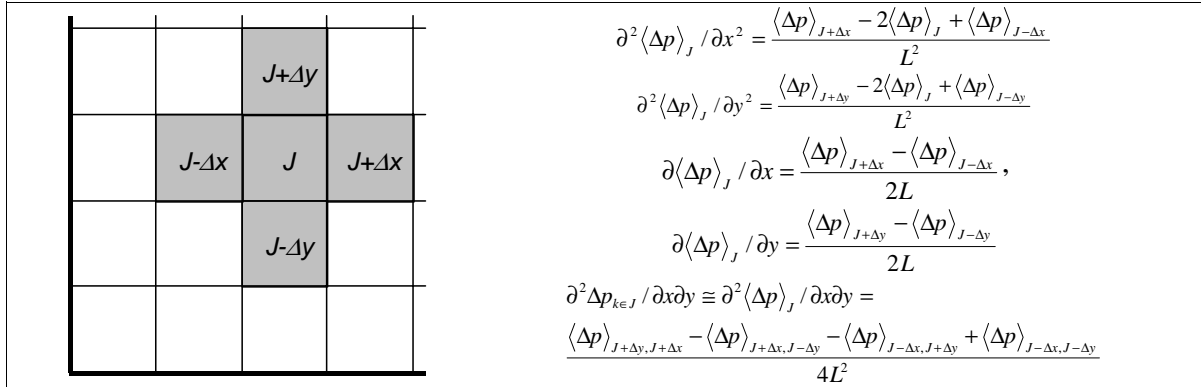


Figure 3 Differentiations on Eulerian square mesh

Equation (10) includes second partial derivatives $\partial^2 \Delta p_k / \partial x^2$, $\partial^2 \Delta p_k / \partial y^2$ and $\partial^2 \Delta p_k / \partial x \partial y$ ($= \partial^2 \Delta p_k / \partial y \partial x$). They are obtained on the Eulerian mesh assuming that Δp_k is uniformly distributed over Cell J . The average excessive pore pressure for Cell J is thus given as:

$$\langle \Delta p \rangle_J = \frac{\sum_{k \in J} V_k \Delta p_k}{\langle V \rangle_J} \quad \text{with} \quad \langle V \rangle_J = \sum_{k \in J} V_k \quad (12)$$

The above second partial derivatives are then obtained on the square Eulerian mesh (**Figure 3**) as:

$$\partial^2 \Delta p_{k \in J} / \partial x^2 \cong \partial^2 \langle \Delta p \rangle_J / \partial x^2 = \frac{\langle \Delta p \rangle_{J+\Delta x} - 2\langle \Delta p \rangle_J + \langle \Delta p \rangle_{J-\Delta x}}{L^2} \quad (13a)$$

$$\partial^2 \Delta p_{k \in J} / \partial y^2 \cong \partial^2 \langle \Delta p \rangle_J / \partial y^2 = \frac{\langle \Delta p \rangle_{J+\Delta y} - 2\langle \Delta p \rangle_J + \langle \Delta p \rangle_{J-\Delta y}}{L^2} \quad (13b)$$

$$\begin{aligned} \partial^2 \Delta p_{k \in J} / \partial x \partial y &\cong \partial^2 \langle \Delta p \rangle_J / \partial x \partial y = \\ &\frac{\langle \Delta p \rangle_{J+\Delta y, J+\Delta x} - \langle \Delta p \rangle_{J+\Delta x, J-\Delta y} - \langle \Delta p \rangle_{J-\Delta x, J+\Delta y} + \langle \Delta p \rangle_{J-\Delta x, J-\Delta y}}{4L^2} \end{aligned} \quad (13c)$$

where, L is the cell size of the Eulerian mesh. Similarly, $\partial \Delta p_k / \partial x$ and $\partial \Delta p_k / \partial y$ for Cell J are:

$$\partial \Delta p_{k \in J} / \partial x \cong \partial \langle \Delta p \rangle_J / \partial x = \frac{\langle \Delta p \rangle_{J+\Delta x} - \langle \Delta p \rangle_{J-\Delta x}}{2L} \quad (13d)$$

$$\partial \Delta p_{k \in J} / \partial y \cong \partial \langle \Delta p \rangle_J / \partial y = \frac{\langle \Delta p \rangle_{J+\Delta y} - \langle \Delta p \rangle_{J-\Delta y}}{2L} \quad (13e)$$

When Cell J is along an impermeable boundary, mirror images of $\langle \Delta p \rangle_J$ are used in Equations (13a)-(13e).

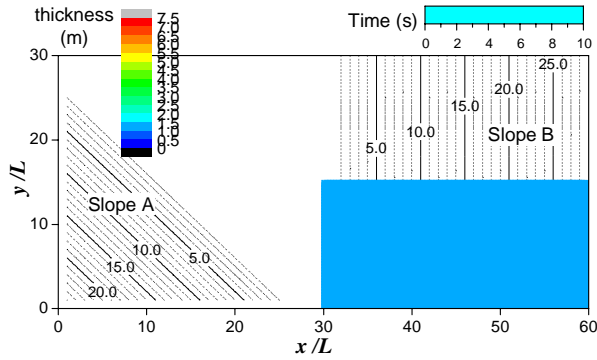
Given the excessive pore pressure Δp_k from Equation (8a), and using Equation (6), pore water pressure P_k is obtained.

NUMERICAL EXAMPLES

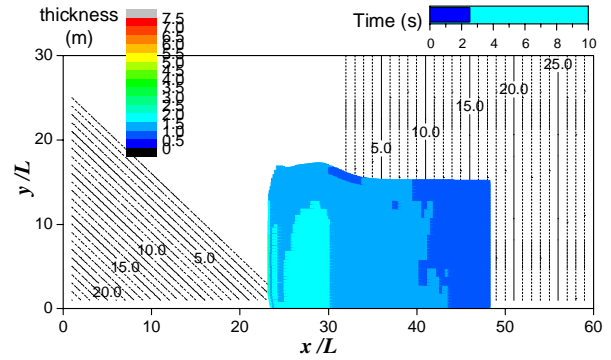
Both the internal friction angles and the cohesions for Lagrangian points were modified to fluctuate randomly around their mean values so that the deviations eventually exhibit the Gaussian distributions. This manipulation is based on the idea that a material exhibiting a complicated hysteresis is comprised of a number of elements exhibiting simple and ideal features ([5, 6]). Parameters (mean values) for the material used in the following example are listed in **Table 1**. Standard deviations of the fluctuated parameters were set at 33% of their mean values.

Table 1. Lagrangian parameters

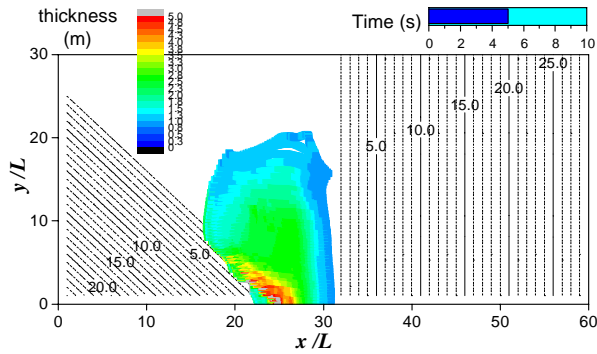
Young's modulus:	$5 \times 10^7 \text{ N/m}^2$	Strength reduction:	Both cohesion and Internal friction angle are reduced by 50%
Poisson's ratio:	0.30	Initial friction angle on the slip surface	0.5 rad
Density:	1700 kg/m^3	u_{ref} in Equation (9)	0.1 m
Internal friction angle:	0.5 rad	\mathcal{A} for local non-viscous damping	0.8
Cohesion:	9800 N/m^2	L: Cell size on x-y plane	



(a) $t = 0 \text{ s}$



(b) $t = 2.5 \text{ s}$



$t = 5 \text{ s}$

Figure 4. Long traveling soil flow:

Contour lines in this figure show that there are two slopes **A** and **B** making up the configuration (see (a)). The soil mass from slope **B** spreads wide as it surged across the horizontal plane, and after hitting Slope **A**, the direction of the mass flow turned avoiding Slope **A**.

The available resistance forces on the slip surface often decreases drastically as the soil mass slips further down because grain crushing causes the buildup of pore water pressure along the slip surface [9]. To reflect this feature of soil, mobilized friction angle $\phi_{i,k}$ for a material point k is assumed to be slip-distance dependent, and given by:

$$\phi_{i,k} = (\phi_{i,k})_{initial} \cdot \exp(-|u_k|/u_{ref}) \quad (5)$$

The slope discussed herein is described as a combination of different planes intersecting each other. The uppermost surfaces of these planes define the slope configuration. **Figures 4a-4c** shows the plan of the slope. Contour lines in this figure show the configuration made of the two slopes **A** and **B**. Diagonal contour lines on the left show that Slope **A** goes diagonally down to the right, while contour lines to the right describe that Slope **B** dips 45 degrees leftward. Lagrangian points are initially arranged in square on Slope **B**. The gravitational acceleration was then given at once to the soil mass, and the mass started sliding down the slope under its own weight. The head of the landslide mass slows down to block the motion of its tail when it reaches the flat land causing the soil at the toe of **Slope B** to be pushed up by the tail. With no lateral confinement on its edge, the soil mass spreads laterally as it surged across the horizontal plane, and after hitting Slope **A**, the direction of the mass flow turned avoiding Slope **A**.

Figure 5 compares two different shapes of the same landslide mass; the former (**Figure 5 (a)**) is the same as that examined in **Figure 4** assuming the landslide mass is dry, while the effect of pore water pressure is taken into account in the latter case (**Figure 5 (b)**). Though the equivalent bulk modulus K was set at 1/1000 of that for water, the built-up pore water pressure was substantially large enough to fluidize the landslide mass, and the mass exhibited more planar shape with a little thinner fringe continuously spreading out, while the dry mass was completely stopped by the soil-breaking slope **B**. **Figure 6** shows the pore water pressure buildup in the landslide mass. The maximum compressive pore water pressure is reached where the landslide mass hits the soil-braking wall.

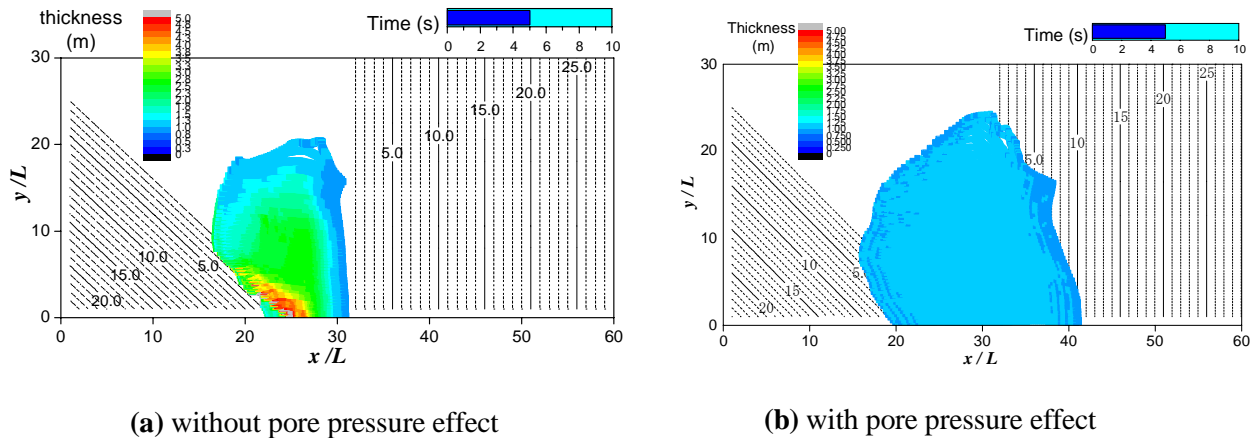


Figure 5. Effect of pore water pressure

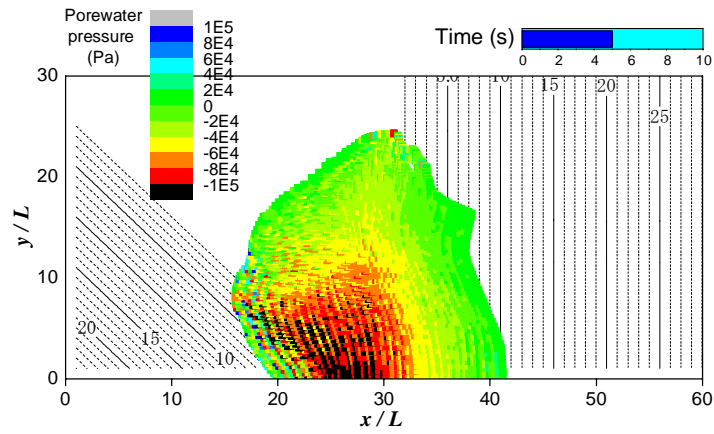


Figure 6. Pore water pressure buildup in landslide mass

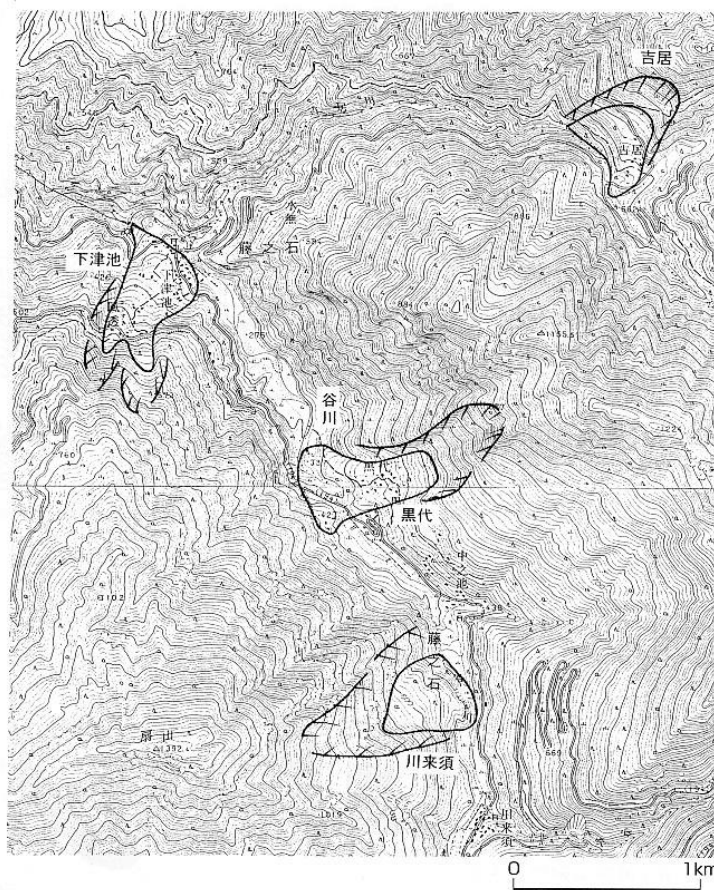


Figure 7. Old landslides along Tanigawa river, Ehime, Japan [7]: Based on ^{14}C dating of suspended matters stopped behind landslide soil masses, these landslides are estimated to have simultaneously taken place about 2050-2150 years ago. Hasegawa [7] conjectures that an earthquake along the Median Tectonic Line triggered them.

SUMMARY AND DISCUSSIONS

The previous example provided a perspective on the capability of the present method for describing long-traveling soil flows. The landslide mass is represented by a plane assembly of soil columns (material points) in contact with each other, free to deform and retaining fixed volumes in their descent down a curving path. The computational mesh can remain constant for the entire computation, thus the main disadvantage of the conventional finite element method related to the problem of mesh distortions is eliminated.

The method however leaves much to improve by comparing these numerical simulations with real examples (see **Figure 7**), and it is extremely difficult to do it, because all Lagrangian parameters for the entire landslide mass are hardly obtained. For example, it is quite often that plants growing on a landslide mass shoot their roots all through the soil mass in such a way that the overall characteristics of the soil mass is largely different from those obtained through conventional soil tests. One possible way will be to consider a real landslide as a huge “simple shear test”. In the “real-size” simple shear test, the distal end and surface configuration of the landslide mass can be clearly measured. If the landslide mass exhibits some liquefiable features, possible peak velocity of the landslide mass will be estimated from mud splatters remaining on walls, tree trunks etc. assuming that they follow forms of parabola [8]. If soil samples are taken from its sliding surface, a rapid simple shear test for example can be conducted for modeling the basal shearing behavior of the soil [9].

Differing from a conventional 2D model for run-out analysis [10], the model proposed herein allows the effect of energy consumption within the deformed landslide mass to be reflected on the numerical evaluation of travel distances. Once a good agreement with a real travel distance is obtained in a landslide-prone area through a parametric study, it is expected the result will provide necessary pieces of information for the landslide risk assessment in this area. An extension of this study will be addressed in future publications.

ACKNOWLEDGMENT: This study was partially granted by APERIF Project, the Special Coordination Fund for Promoting Science and Technology of the Ministry of Education, Culture, Sports, Science and Technology, Japan.

REFERENCES

1. Cundall, P.A. and Board, M. “A microcomputer program for modeling large-strain plasticity problems.” Numerical Methods in Geotechnics (Proc., 6th Int. Conf., Innsbruck, Austria, April 1988), 2101-2108, 1988.
2. Sulsky, D., Z., Chen, and H. L., Schreyer, “A particle method for history dependent materials.” Comput. Methods Appl. Mech. Engrg. 1994; 118: 179-196.
3. Konagai, K. and Johansson, J. “Two Dimensional Lagrangian Particle Finite Difference Method for Modeling Large Soil Deformations.” Structural Eng./ Earthquake Eng. 2001; 18(2): 91s-95s.
4. Konagai, K. and Numada, M. “Pseudo-three dimensional Lagrangian Particle Finite Difference Method for modeling long-traveling soil flows.” Journal of Japan Society of Dam Engineers 2002; 12(2): 123-128.

5. Iwan, W.D. "A distributed-element model for hysteresis and its steady-state dynamic response." *Jour., Appl. Mechanics* 1966; pp. 893-900.
6. Ogawa, Y. "A model for hysteresis of soil and its steady-state strain energy and energy loss." *Proc. 6th Japan Earthquake Engineering Symp.*, 529-536, 1982.
7. Hasegawa S. "Landslide-created reservoirs, Geomorphology for mountains." *Japan Society of Engineering Geology, Kokon-shoin*, 63-65, 2000.
8. Konagai, K. et al. "Las Colinas landslide caused by the January 13, 2001 Off the Coast of El Salvador Earthquake." *Journal of Japan Association for Earthquake Engineering* 2002; 2(1), 1-15.
9. Sassa, K. "Prediction of earthquake induced landslides." *Special Lecture, 7th Intern., Symp., Landslides, Balkema, Rotterdam*, 1, 115-132, 1996.
10. Hungr, O. "A model for runout analysis of rapid flow slides, debris flows and avalanches." *Canadian Geotechnical Journal* 1995, 32, 610-625.